THE JOURNAL OF PHYSICAL CHEMISTRY Letters

Letter

Cite This: J. Phys. Chem. Lett. 2018, 9, 6915−6920

pubs.acs.org/JPCL

Interlayer-Decoupled Sc-Based Mxene with High Carrier Mobility and Strong Light-Harvesting Ability

Liujiang Zhou,*[,†,‡] Yu Zhang,[†] Zhiwen Zhuo,[¶] Amanda J. Neukirch,[†] and Sergei Tretiak*[,‡,§,†]

[†]Theoretical Physics and Chemistry of Materials, Los Alamos National Laboratory, Los Alamos, New Mexico 87545, United States

[‡]Center for Nonlinear Studies, Los Alamos National Laboratory, Los Alamos, New Mexico 87545, United States

[§]Hefei National Laboratory of Physical Sciences at the Microscale, University of Science and Technology of China, Hefei, Anhui 23026, China

[¶]Center for Integrated Nanotechnologies, Los Alamos National Laboratory, Los Alamos, New Mexico 87545, United States

Supporting Information

ABSTRACT: Two-dimensional (2D) van der Waals (vdW) layered materials offer a unique combination of electronic and structural properties attractive for technological applications. Most of them show strong vdW interactions, which lead to interlayer-coupled optoelectronic properties due to quantum confinement. Here we present a systematic computational study of one Mxene, 2D double-metal-layered scandium chloride carbides (Sc_2CCl_2). Unlike conventional quantum-confined nanosystems, 2D Sc_2CCl_2 exhibits weak vdW interactions with robust interlayer-decoupled optoelectronic properties and extremely high and anisotropic carrier mobilities of about $1-4.5 \times 10^4$ cm^2 V^{-1} s^{-1} that consequently produce comparatively large drain currents. Specifically, the 2D Sc_2CCl_2 family has strong light-harvesting ability and could be utilized as efficient donor materials in excitonic solar cells. Overall, in combination with high structural stability against ambient conditions, interlayer-decoupled robust optoelectronic properties potentially relax the requirements for the fabrication of high-quality monolayers and for selection of suitable substrates and suggest promising next-generation optoelectronic applications.

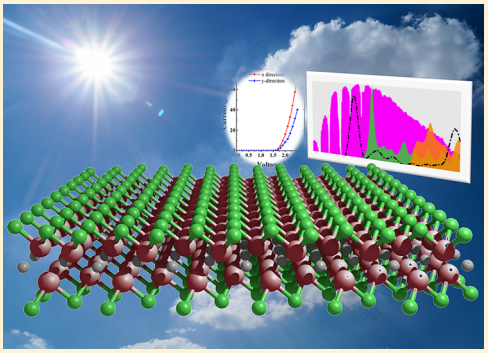

Two-dimensional (2D) van der Waals (vdW) layered materials have been a subject of intense studies and shown wide applications for the past decade.[1−5] Although conventional 2D materials exhibit exotic phenomena, they suffer from some intrinsic drawbacks. For example, graphene has extremely high carrier mobilities due to the existence of a massless Dirac cone and thus holds promise for high-speed field effect transistor (FET) devices.[6,7] Unfortunately, the vanishing energy gap greatly limits its widespread application in this field.[8] The prototype 2D transition metal dichalcogenides (TMDs), monolayer molybdenum disulfide (MoS_2), is a direct-band-gap semiconductor. However, its small carrier mobility, which is (60−200 cm^2 V^{-1} s^{-1})[9,10] several orders of magnitude lower than that of graphene,[6,7] is prohibitive for practical applications. Black phosphorus with a unique puckered structure exhibits an inherently moderate band gap[11] and an increased carrier mobility (10^3 cm^2 V^{-1} s^{-1}).[11] Yet, black phosphorus-based electronic devices undergo rapid performance degradation when exposed to air due to the chemical instability of the material.[12] These situations call for a need to explore 2D semiconductors that exhibit a moderate energy gap, high carrier mobility and light-harvesting ability, stability at ambient conditions, as well as feasible experimental access.

Within 2D vdW layered materials, the interlayer coupling is primarily driven by vdW interactions. Most 2D materials have strong vdW interactions, standing for significant interlayer coupling, which results in thickness-dependent electronic structures due to varying quantum confinement.[11,13] Such strong coupling challenges fabrication routes to prepare precisely defined single-crystal monolayers and/or multilayers to attain desired electronic structures, let alone the large-scale synthesis required for a wide use.[14] In the opposite limit, 2D materials with weak vdW interactions may have an essentially single-layer defined electronic structure insensitive to a bulk composition or an interlayer-decoupled property. Importantly, such weak vdW interactions greatly relax synthetic requirements for preparing uniform single-crystal monolayers and avoid the negative impacts on monolayers from the substrate effect and thus suggest future applications at low cost. Tongay et al.[14] reported that the electronically and vibrationally decoupled effects could be realized in a 2D ReS_2 crystal, which has similar band gaps across a variety of multilayer structures. Nevertheless, this contradicts observed strong interlayer

Received: October 6, 2018
Accepted: November 24, 2018
Published: November 24, 2018

DOI: 10.1021/acs.jpclett.8b03077
J. Phys. Chem. Lett. 2018, 9, 6915−6920

vibrational modes in bulk ReS_2[15] and recently measured optical absorption,[16] photoluminescence,[17] photoemission,[18] and transport behavior[19] of ultrathin crystals, which demonstrates thickness dependence of the electronic and optical properties. Consequently, the true electronically interlayer-decoupled system is yet to be observed. Zha et al.[20] reported that 2D Sc_2CF_2 displays high carrier mobility (up to 5×10^3 $cm^2\ V^{-1}\ s^{-1}$), but the large gap (above 2.0 eV)[21] prohibits its applications for FETs and solar cells. A similar 2D Sc_2CCl_2 material may have a smaller gap and superior electronic properties. Given that a homologous layered compound of a Sc_2CCl_2 bulk crystal was successfully synthesized a while ago,[22] this material may finally address the above demands for future optoelectronic devices.

In this Letter, we subject 2D Sc_2CCl_2 to a broad range of ab initio calculations outlined in the Methods section. We find that 2D Sc_2CCl_2 has unusually weak vdW interactions and interlayer-decoupled electronic, transport, and optical properties. Here the vdW interaction is caused by the large electronegativity of Cl atomic planes and the vanishing wave function overlap around the Fermi level. This strongly contrasts conventional 2D materials showing strong vdW interactions with interlayer-coupled properties. Moreover, 2D Sc_2CCl_2 also features highly anisotropic carrier mobility of $1-4.5 \times 10^4$ $cm^2\ V^{-1}\ s^{-1}$, which consequently leads to comparatively large drain currents. The calculated optical absorbance spectrum of 2D Sc_2CCl_2 further reveals the promising light-harvesting ability with interlayer-decoupled optical band gaps of about 1.52 eV. Importantly, such weak vdW interactions could greatly relax the requirements for the fabrication of high-quality monolayers and for the selection of suitable substrates in future experimental and industry exploration.

In the calculations of geometry optimization, electronic structures were performed using the Vienna ab initio simulation package (VASP).[23] The phonon calculations were carried out using finite displacements as implemented in the PHONOPY code.[24] The derivatives of macroscopic dielectric tensors with respect to the normal-mode coordinate were computed so as to obtain the off-resonance Raman activities of vibrational modes.[25] The carrier mobility (μ) was obtained in the framework of the deformation potential (DP) theory.[26,27] The quantum transport properties were simulated via the nonequilibrium Green's function (NEGF) formalism, and the current flowing through the device was evaluated via the Landauer–Buttiker formula.[28,29] The GW calculations were performed without self-consistency in the Green's function and the screened Coulomb interaction (G0W0 approximation) in combination with the random phase approximation (RPA) or Bethe–Salpeter equation (BSE) calculations to calculate the quasi-particle band gap and the light absorbance with or without electron–hole (e–h) interactions, as implemented in YAMBO code.[30] The methods and computational details are presented in the Supporting Information.

The layered Sc_2CCl_2 crystal has two phases, e.g., 1T ($P\bar{3}m1$) and 3R ($R\bar{3}m$) phases of Sc_2CCl_2, as observed in experiment.[22] Our calculations show that the 3R phase is more stable and energetically favorable by about 0.09 eV per formula unit compared to the 3R one, which is also in line with the experimental observation.[22] We therefore only consider the 1T phase of Sc_2CCl_2 in this work. The bulk and one-layer (1L) crystal structures of Sc_2CCl_2 are shown in Figure 1a–c. The bulk phase crystallizes in the trigonal space group $P\bar{3}m1$, in

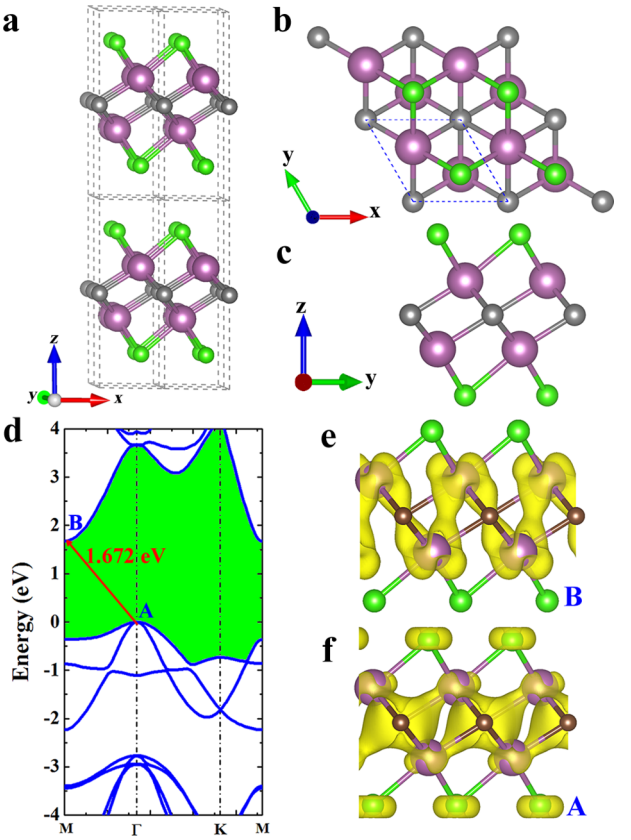

Figure 1. (a) Crystal structure of bulk Sc_2CCl_2: purple, gray and green balls are Sc, C, and Cl atoms, respectively. (b) Top and (c) side views of 1L Sc_2CCl_2. The blue dashed line in (b) denotes the unit cell. (d) Band structure of 1L Sc_2CCl_2 calculated based on HSE06. The Fermi level is shifted to the VBM. Isosurface (0.006 e/Å^3) of partial charge densities at (e) A and (f) B points in the plot (d). A and B points are the VBM and CBM, respectively.

which the Sc_2C plane is halogenated by two Cl atomic layers in a bridge-coordinating way. The calculated lattice constants via structural optimization for bulk and 1L Sc_2CCl_2 are almost identical with $a = b = 3.42$ Å, close to the experimental values of 3.40 Å in the bulk phase.[22] In 1L Sc_2CCl_2, one atomic layer of C atoms is shrouded by two Sc atomic layers that are halogenated by two layers of Cl atoms on each side. The central C atoms are octahedrally coordinated to six Sc atoms. In the Sc_6C octahedron, the six Sc–C bonds display an almost identical bond length of 2.328 Å. The phonon spectrum (Figure S1) shows that all phonon branches are positive across the entire Brillouin zone (BZ), indicating phase stability without any dynamical instability in 1L Sc_2CCl_2. We also performed the ab initio molecular dynamics under an *NVT* ensemble for about 6 ps at 300 K. The results show no signs of structural disruption and suggest the high thermal stability for 2D Sc_2CCl_2 (Figure S2).

The 1L Sc_2CCl_2 is an indirect-band-gap semiconductor with a band gap of 0.840 eV (PBE level) or 1.672 eV (HSE06 level). The valence band maximum (VBM) and conduction band minimum (CBM) are located at the Γ and M points, respectively, in the BZ (Figure 1d). The VBM consists of hybridized p–d orbitals from Sc-d states (mainly d_{xy} and d_{x^2}) and p states (mainly p_x and p_y) of C and Cl atoms, and the CBM mostly consists of Sc-d orbitals (mainly d_{xz} and d_{yz}) (see Figure 1e,f). According to Bader charge analysis,[31] the Sc

DOI: 10.1021/acs.jpclett.8b03077
J. Phys. Chem. Lett. 2018, 9, 6915–6920

atoms lose 1.54 electrons per atom, whereas Cl and C atoms gain 0.63 and 1.83 electrons per atom, respectively, coinciding with the difference charge density shown in Figure S3. The electron localization function (ELF) (Figure S4) also shows that there is very little electron localization between Sc−C and Sc−Cl bonds, reflecting that ionic bond character is dominant in Sc_2CCl_2, similar to a monolayer Tl_2O.[32] Table 1 summarizes

Table 1. Calculated DP Constant (E_1), 2D Elastic Modulus (C_{2D} in units of N/m), Effective Mass (m^* in units of m_e), and Mobility (μ in units of $cm^2\ V^{-1}\ s^{-1}$) for Electrons (e) and Holes (h) along the x and y Directions in the 2D 1L Sc_2CCl_2 at 300 K

N_L	carrier type	E_1	C_{2D}	m^*	μ
1L	e(x)	1.17	158.9	0.23	19277
	h(x)	1.88	158.9	0.685	1127
	e(y)	1.19	161.1	1.319	3351
	h(y)	1.79	161.1	2.260	380
2L	e(x)	1.07	311.9	0.231	45342
	h(x)	2.05	311.9	0.412	4437
	e(y)	1.04	316.7	1.337	8421
	h(y)	2.03	316.7	1.809	1047
3L	e(x)	1.40	475.8	0.232	40457
	h(x)	1.76	475.8	0.379	10227
	e(y)	1.34	479.8	1.325	7806
	h(y)	1.76	479.8	1.887	2074

the variations in geometries as a function of the layer number from 1 to 3. The lattice parameter a remains the same value (3.42 Å) when passing from bulk to 1L Sc_2CCl_2, whereas the Sc−C and Sc−Cl bond lengths grow by 0.006 and 0.003 Å, respectively. All thicker few-layer structures retain semiconducting features and have nearly identical band dispersions to that of the 1L Sc_2CCl_2. Few-layer and bulk Sc_2CCl_2 have weakly varying band gaps of 0.796−0.84 eV (PBE level) or 1.63−1.672 eV (HSE06 level) when going from bulk to 1L (Figure 2 and Table S1), suggesting the existence of interlayer-decoupled electronic structure in few-layer and bulk Sc_2CCl_2. This is in stark contrast to conventional 2D materials, where band structures are strongly dependent on the number of layers.[33,34]

The carrier mobilities (μ) were obtained in the framework of DP theory.[26,27] An orthogonal supercell model of the 1L structure was built (Figure 2e) to give intuitive variations of carrier mobilities. The band structure of the orthogonal model shows a direct band gap with the CBM and VBM located at the same Γ point (Figure 2f). This suggests that a direct interband tunnel FET could be realized without relying on the phonon-assisted optical transitions. As listed in Table 1, the electron effective masses along x and y are 0.23 and 1.32 m_e, respectively, smaller than those for holes (0.685 and 2.26 m_e). The low effective mass for the electron is attributed to the strong band dispersion in the CB, which is associated with the weakly varying atomic potential within the Sc_2C plane.[32] The 2D elastic moduli in x and y directions are 158.9 and 160.1 N/m, respectively, stemming from the nearly identical energy response in the two directions when subject to uniaxial strain (Figure S5a,b). The obtained DPs for electrons and holes are 1.18−1.19 and 1.79−1.88 eV, respectively, significantly smaller than those in monolayer MoS_2 (5.3−11.4 eV),[35] graphene (5.0 eV),[36] and h-BN (3.67).[37] Such small E_1 values can be interpreted well by the extremely low overlap between real-space charge distributions of the VBM and CBM (Figure 1e,f). These above features finally produce the high and anisotropic carrier mobilities of 1.9×10^4 and 1×10^3 $cm^2\ V^{-1}\ s^{-1}$ for electrons and holes along x directions, respectively. The carrier mobilities in 2L and 3L Sc_2CCl_2 are in general significantly larger while retaining similar traits compared to the 1L Sc_2CCl_2. Except for the elastic modulus C's monotonous increase as a function of the number of layers (Table 1 and Figure S6), the potential constant (E_1) in two directions has an almost constant value of about 1.07−1.40 and 1.76−2.05 for electrons and holes, respectively. The increase of E_1 in 2L and 3L structures is less than 0.5 relative to that of the 1L structure, displaying layer-independent features. It should be noted that when going from 2L to 3L, C_{2D} and E_1 for electrons have 1.5- and 1.30-fold increases, respectively, finally producing relatively unchanged electron mobility. The largest carrier mobilities are 4.5×10^4 and 1.0×10^4 $cm^2\ V^{-1}\ s^{-1}$ for electrons and holes, respectively, along the x direction. High carrier mobilities usually produce large drain currents in FET devices, as supported in our calculations of transport properties by the NEGF formalism (see the Methods section and Figures S7 and S8 in the Supporting Information). These large carrier mobility and drain currents suggest the potential applications of 2D Sc_2CCl_2 in high-speed electronic devices.

We also predicted the optical absorption spectra of few-layer Sc_2CCl_2 by conducting the GW calculations to determine both the quasi-particle band gap and the light absorbance as described in the Methods in the Supporting Information. Figure 3 shows that their G_0W_0 gaps are 2.10, 1.98, 1.94, and 1.55 eV, for 1L, 2L, 3L, and bulk structures, respectively, about 0.2 eV lower than the onset edges of light absorption based on GW + RPA for few-layer Sc_2CCl_2. This phenomenon could be originated from the transition rule. The VBM at Γ and CBM at M possess the same parity of −1, leading to a forbidden electronic transition between them. The allowed lowest transitions are found at the M point with a direct transition of 2.27, 2.19, 2.16, and 1.72 eV for few-layer and bulk systems (Table S1), respectively. The first prominent optical absorption peaks (defined as the optical band gap) for all studied systems are located at about 1.52 eV (Figures 3 and S9), corresponding to excitons with binding energies (E_b) of 0.75, 0.67, and 0.63 eV for 1L, 2L, and 3L Sc_2CCl_2, respectively. Similar to other 2D systems, large exciton binding energies arise from the reduced screening in low-dimensional systems. This optical band gap remains constant with a change in thickness, displaying light absorption independence to the number of layers. The final optical band gap in the bulk phase resides at about 1.66 eV, only about 0.14 eV larger than those in few-layer Sc_2CCl_2.

To evaluate the light-harvesting ability, we calculated the absorbed photon flux (J_{abs}) for the 2D Sc_2CCl_2 family (see details in the Supporting Information). The obtained J_{abs} values of 1L, 2L, and 3L structures are 1.32, 4.51, and 7.80 mA/cm^2. There numbers are comparable to and higher than those for siligraphene[38,39] (2.32−2.70 mA/cm^2) and phosphorene (1.12−2.38 mA/cm^2)[40] with an artificially specified layer thickness Δz of about 1 nm. As for the bulk phase, the absorbance for a flat layer of thickness Δz = 1 nm using $A = 1 - e^{-\alpha \cdot \Delta z}$ is 4.78 mA/cm^2. This is generally higher compared to 1 nm thick representative bulk materials of relevance, such as crystalline Si (0.1 mA/cm^2) and GaAs (0.3 mA/cm^2).[41] These J_{abs} values demonstrate that the 2D Sc_2CCl_2 family has strong light absorption in the visible region (390−700 nm),

DOI: 10.1021/acs.jpclett.8b03077
J. Phys. Chem. Lett. 2018, 9, 6915−6920

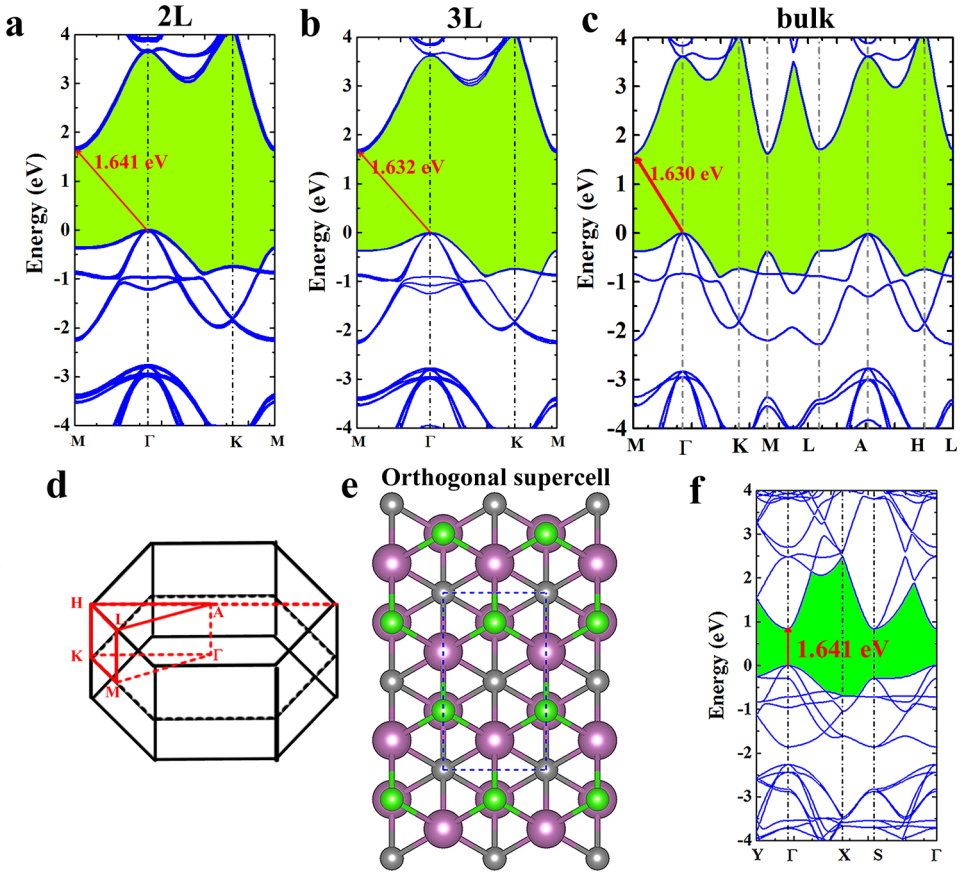

Figure 2. Band structures of (a) bilayer (2L), (b) trilayer (3L), and (c) bulk Sc_2CCl_2 with primitive unit cells based on the HSE06 level. Few-layer band structures are plotted along the high-symmetry lines M−Γ−K−M, and those of bulk phases are presented along the high-symmetry lines M−Γ−K−M−L−A−H−L in the BZ. The Fermi level is set to zero. The indirect band gaps of the primitive cell are indicated by red lines. (d) Associated BZ of the bulk phase. (e) Rectangular supercell of the 1L Sc_2CCl_2 with a unit cell labeled by the blue dashed line. (f) Band structure of the rectangular supercell of 1L Sc_2CCl_2, where the transition of the indirect−direct band gap is realized by band folding from M to Γ. The direct band gap with the CBM and VBM located at the same Γ point is also indicated by the red line.

suggesting that 2D Sc_2CCl_2 compounds would be superior light absorbers in excitonic solar cells. If paired with suitable acceptors with matching band alignments, one can envision Sc_2CCl_2-based excitonic solar cells. Further studies of these optoelectronic devices are ongoing.

Our simulations have shown that 2D Sc_2CCl_2 exhibits interlayer-decoupled electronic, transport, and optical properties. This feature could be ascribed to the weak vdW interactions. We calculated the interlayer coupling energy of the bilayer structure to be about 5 meV (PBE level in the absence of vdW correction) or 95 meV (DFT-D2 level with vdW terms (Figure S10a), see the Methods in the Supporting Information) per unit cell. This is smaller than that of already synthesized 2D ReS_2 crystals (18 meV, PBE level)[14] and far smaller than that of MoS_2 [(58 meV, PBE level) in ref 14 and 42 meV (PBE level, this work) or 149 meV (DFT-D2 level)]. If we describe the interlayer coupling energy with respect to contributing atoms, 2D Sc_2CCl_2 has a binding energy of about 9 meV per atom, which is about 3 times smaller than that of bilayer MoS_2 (25 meV). Such weak interlayer coupling energy leads to the decoupling of lattice vibrations between adjacent layers in Sc_2CCl_2, as supported by our calculated Raman spectrum in Figure S10b. Such weak vdW interactions are rationalized by the following two factors: (1) The large electronegativity of Cl atoms leads to the "hard" outer layer of Cl atoms with contracted electron clouds and weak polarization and further lessens the dipole-induced interlayer interactions; (2) vanishing wave function overlap around the Fermi level appears in both bulk and multilayer structures, as shown in Figure 4, which produces the electronically insensitive nature between interacting Sc_2CCl_2 layers. Thus, 2D Sc_2CCl_2 has interlayer-decoupled electronic structures, nearly constant values of the DPs, and exciton peaks at about 1.52 eV in both bulk and multilayer structures, standing in contrast to conventional quantum-confined nanosystems. Switching to the other two homologous halides Sc_2CX_2 (X = Br, I) and owing to the fact that halogen atoms have Cl > Br > I order of electronegativity, we expect the increase of weak vdW interactions and the reduction of the interlayer-decoupled feature from Sc_2CCl_2 to Sc_2CBr_2 and to Sc_2CI_2.

Experiments on conventional 2D systems are also usually limited by the availability of large-area monolayers or by high sensitivity to material thickness or by tightened restrictions of suitable substrates. In contrast, the weak vdW interactions successfully enable straightforward experimental access and relax synthetic requirements for preparing large-area, single-crystal monolayers and for selection of suitable substrates. Therefore, 2D Sc_2CCl_2 serves as a promising platform to probe 2D excitonic and lattice physics at low cost. Moreover, the outer Cl atomic layers could provide experimental access of 2D Sc_2CCl_2 via chlorination over a bare Sc_2C monolayer. Our ELF calculations verified that the inner Sc_2C layer has a metal

DOI: 10.1021/acs.jpclett.8b03077
J. Phys. Chem. Lett. 2018, 9, 6915−6920

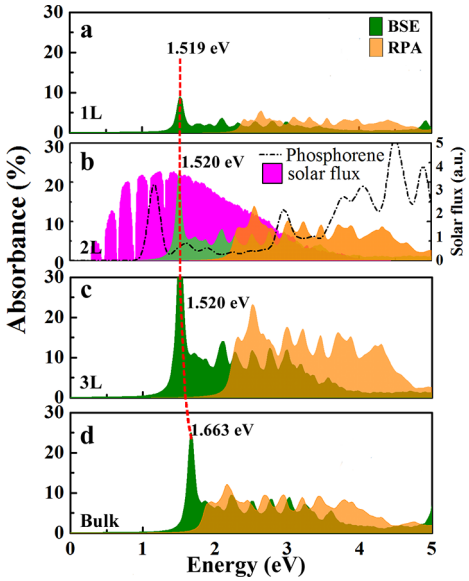

Figure 3. Optical absorbance spectra of few-layer (a–c) and bulk (d) Sc_2CCl_2 for light incident in the z direction and polarized along the in-plane direction. The light absorbances are calculated based on GW + RPA (green) and GW + BSE (yellow) levels for including and excluding e–h interactions, respectively. Red dashed lines show the evolution of the first optical peak as a function of the material thickness. In panel (b), the absorbance of phosphorene along the armchair direction is also presented with those of 2L Sc_2CCl_2, which are overlapped with the incident AM1.5G solar flux to reflect the ability of light harvesting.

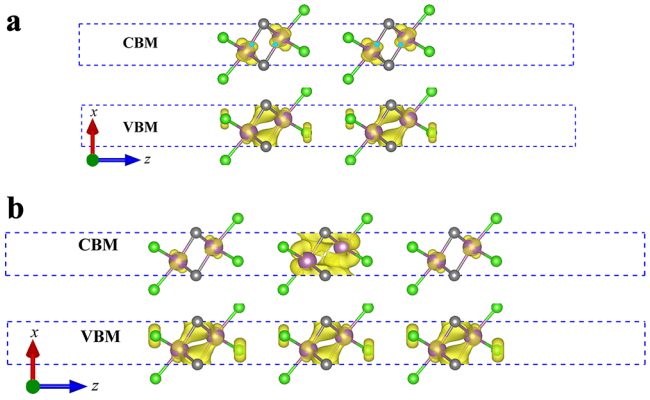

Figure 4. (a) Spatial structure of wave functions for the VBM and CBM in 2L Sc_2CCl_2, using an isosurface of 0.004 e/Å^3. (b) Spatial structure of wave functions for the VBM and CBM in 3L Sc_2CCl_2, using an isosurface of 0.002 e/Å^3.

feature with 2D electride states delocalized above both surfaces of the Sc_2C plane (Figure S11). Due to traits of the bare Sc metal atomic layer and anionic electride states, the Sc_2C sheet is highly sensitive to oxygen or water contamination. We calculated the adsorption energies of isolated O atoms and H_2O molecules on 1L Sc_2CCl_2 to evaluate chemical stability when exposed to air. The obtained adsorption energy for an isolated O atom is 2.56 eV/atom, being higher than that on phosphorene (about 2.1 eV/atom), suggesting the higher inertia to oxidation. The adsorption energy of a single H_2O is −0.11 eV/molecule, being smaller than that of phosphorene (−0.187 eV/molecular), indicating better robustness against humidity.[42]

In conclusion, using first-principles calculations, we have computationally studied the optoelectronic properties of Sc-based Mxene materials of 2D double-metal-layered Sc_2CCl_2. We show that 2D Sc_2CCl_2 displays weak vdW interactions. These weak interlayer interactions ensure intrinsic interlayer-decoupled optoelectronic properties and allow one to bypass the strict requirements for the preparation of high-purity monolayers and for selection of suitable substrates. Specifically, we attribute this unusual feature to the large electronegativity of Cl atoms and vanishing wave function overlap around the Fermi level. In combination with the anisotropic effective masses and monotonically increasing elastic modulus, 2D Sc_2CCl_2 exhibits comparatively high and anisotropic carrier mobility of up to 4.5×10^4 and 1.0×10^4 cm^2 V^{-1} s^{-1} for electrons and holes, respectively. The calculated electronic and optical features suggest that Sc_2CCl_2 is also a promising donor material for light harvesting in solar cells. In addition, 2D Sc_2CCl_2 could be experimentally accessible via mechanical exfoliation from its corresponding 3D bulk phase and has high structural stability against ambient conditions. Overall, these results suggest the high feasibility of 2D Sc_2CCl_2 for high-speed electronic and photovoltaic applications.

■ ASSOCIATED CONTENT

Supporting Information

The Supporting Information is available free of charge on the ACS Publications website at DOI: 10.1021/acs.jpclett.8b03077.

Calculations of interlayer coupling energy and absorbed photo flux, phonon spectrum, snapshots of molecular dynamics simulation, difference charge density, electron localization function, snapshots of molecular dynamics simulation total energy–strain curve, illustration of two-probe systems for 1L Sc_2CCl_2, frequency-dependent dielectric function, interlayer coupling energy and Raman spectra, electron localization function of the 1L Sc_2C plane (PDF)

Crystallographic files of all calculated structures (ZIP)

■ AUTHOR INFORMATION

Corresponding Authors

*E-mail: ljzhou86@lanl.gov (L.Z.).
*E-mail: serg@lanl.gov (S.T.).

ORCID

Liujiang Zhou: 0000-0001-5814-4486
Yu Zhang: 0000-0001-8938-1927
Sergei Tretiak: 0000-0001-5547-3647

Notes

The authors declare no competing financial interest.

■ ACKNOWLEDGMENTS

This work was supported by the U.S. Department of Energy through the Los Alamos National Laboratory (LANL). LANL is operated by Triad National Security, LLC, for the National Nuclear Security Administration of the U.S. Department of Energy (Contract No. 89233218NCA000001). This work was done in part at the Center for Nonlinear Studies (CNLS) and the Center for Integrated Nanotechnologies CINT) at LANL. This research used resources provided by the LANL Institutional Computing Program.

DOI: 10.1021/acs.jpclett.8b03077
J. Phys. Chem. Lett. 2018, 9, 6915–6920

REFERENCES

(1) Duong, D. L.; Yun, S. J.; Lee, Y. H. van der Waals Layered Materials: Opportunities and Challenges. *ACS Nano* **2017**, *11*, 11803−11830.

(2) Long, M.; Gao, A.; Wang, P.; Xia, H.; Ott, C.; Pan, C.; Fu, Y.; Liu, E.; Chen, X.; Lu, W.; et al. Room temperature high-detectivity mid-infrared photodetectors based on black arsenic phosphorus. *Sci. Adv.* **2017**, *3*, No. e1700589.

(3) Klein, D. R.; MacNeill, D.; Lado, J. L.; Soriano, D.; Navarro-Moratalla, E.; Watanabe, K.; Taniguchi, T.; Manni, S.; Canfield, P.; Fernández-Rossier, J.; et al. Probing magnetism in 2D van der Waals crystalline insulators via electron tunneling. *Science* **2018**, *360*, 1218−1222.

(4) Jariwala, D.; Marks, T. J.; Hersam, M. C. Mixed-dimensional van der Waals heterostructures. *Nat. Mater.* **2017**, *16*, 170−181.

(5) Wilson, N. R.; Nguyen, P. V.; Seyler, K.; Rivera, P.; Marsden, A. J.; Laker, Z. P. L.; Constantinescu, G. C.; Kandyba, V.; Barinov, A.; Hine, N. D. M.; et al. Determination of band offsets, hybridization, and exciton binding in 2D semiconductor heterostructures. *Sci. Adv.* **2017**, *3*, No. e1601832.

(6) Liao, L.; Lin, Y.-C.; Bao, M.; Cheng, R.; Bai, J.; Liu, Y.; Qu, Y.; Wang, K. L.; Huang, Y.; Duan, X. High-speed graphene transistors with a self-aligned nanowire gate. *Nature* **2010**, *467*, 305−308.

(7) Schwierz, F. Graphene transistors. *Nat. Nanotechnol.* **2010**, *5*, 487−496.

(8) Novoselov, K. S.; Geim, A. K.; Morozov, S. V.; Jiang, D.; Katsnelson, M. I.; Grigorieva, I. V.; Dubonos, S. V.; Firsov, A. A. Two-dimensional gas of massless Dirac fermions in graphene. *Nature* **2005**, *438*, 197−200.

(9) Radisavljevic, B.; Radenovic, A.; Brivio, J.; Giacometti, V.; Kis, A. Single-layer MoS2 transistors. *Nat. Nanotechnol.* **2011**, *6*, 147.

(10) Fuhrer, M. S.; Hone, J. Measurement of mobility in dual-gated MoS2 transistors. *Nat. Nanotechnol.* **2013**, *8*, 146−147.

(11) Li, L.; Yu, Y.; Ye, G. J.; Ge, Q.; Ou, X.; Wu, H.; Feng, D.; Chen, X. H.; Zhang, Y. Black phosphorus field-effect transistors. *Nat. Nanotechnol.* **2014**, *9*, 372−377.

(12) Ziletti, A.; Carvalho, A.; Campbell, D.; Coker, D.; Castro Neto, A. Oxygen defects in phosphorene. *Phys. Rev. Lett.* **2015**, *114*, No. 046801.

(13) Liu, H.; Du, Y.; Deng, Y.; Ye, P. D. Semiconducting black phosphorus: synthesis, transport properties and electronic applications. *Chem. Soc. Rev.* **2015**, *44*, 2732−2743.

(14) Tongay, S.; Sahin, H.; Ko, C.; Luce, A.; Fan, W.; Liu, K.; Zhou, J.; Huang, Y.-S.; Ho, C.-H.; Yan, J.; et al. Monolayer behaviour in bulk ReS_2 due to electronic and vibrational decoupling. *Nat. Commun.* **2014**, *5*, 3252.

(15) Qiao, X.-F.; Wu, J.-B.; Zhou, L.; Qiao, J.; Shi, W.; Chen, T.; Zhang, X.; Zhang, J.; Ji, W.; Tan, P.-H. Polytypism and unexpected strong interlayer coupling in two-dimensional layered ReS_2. *Nanoscale* **2016**, *8*, 8324−8332.

(16) Aslan, O. B.; Chenet, D. A.; van der Zande, A. M.; Hone, J. C.; Heinz, T. F. Linearly Polarized Excitons in Single- and Few-Layer ReS_2 Crystals. *ACS Photonics* **2016**, *3*, 96−101.

(17) Zhao, H.; Wu, J.; Zhong, H.; Guo, Q.; Wang, X.; Xia, F.; Yang, L.; Tan, P.; Wang, H. Interlayer interactions in anisotropic atomically thin rhenium diselenide. *Nano Res.* **2015**, *8*, 3651−3661.

(18) Gehlmann, M.; Aguilera, I.; Bihlmayer, G.; Nemšák, S.; Nagler, P.; Gospodarič, P.; Zamborlini, G.; Eschbach, M.; Feyer, V.; Kronast, F.; et al. Direct Observation of the Band Gap Transition in Atomically Thin ReS_2. *Nano Lett.* **2017**, *17*, 5187−5192.

(19) Ovchinnikov, D.; Gargiulo, F.; Allain, A.; Pasquier, D. J.; Dumcenco, D.; Ho, C.- H.; Yazyev, O. V.; Kis, A. Disorder engineering and conductivity dome in ReS_2 with electrolyte gating. *Nat. Commun.* **2016**, *7*, 12391.

(20) Zha, X.-H.; Zhou, J.; Zhou, Y.; Huang, Q.; He, J.; Francisco, J. S.; Luo, K.; Du, S. Promising electron mobility and high thermal conductivity in Sc_2CT_2 (T = F, OH) MXenes. *Nanoscale* **2016**, *8*, 6110−6117.

(21) Jiang, Z.; Liu, Z.; Li, Y.; Duan, W. Scaling universality between band gap and exciton binding energy of two-dimensional semiconductors. *Phys. Rev. Lett.* **2017**, *118*, 266401.

(22) Hwu, S. J.; Ziebarth, R. P.; Von Winbush, S.; Ford, J. E.; Corbett, J. D. Synthesis and structure of double-metal-layered scandium, yttrium, and zirconium chloride carbides and nitrides, M_2Cl_2C and M_2Cl_2N. *Inorg. Chem.* **1986**, *25*, 283−287.

(23) Kresse, G.; Furthmuller, J. Efficient iterative schemes for *ab initio* total-energy calculations using a plane-wave basis set. *Phys. Rev. B: Condens. Matter Mater. Phys.* **1996**, *54*, 11169−11186.

(24) Togo, A.; Tanaka, I. First principles phonon calculations in materials science. *Scr. Mater.* **2015**, *108*, 1−5.

(25) Fonari, A.; Stauffer, S. *vasp_raman.py*. https://github.com/raman-sc/VASP/ (2013).

(26) Bardeen, J.; Shockley, W. Deformation potentials and mobilities in non-polar crystals. *Phys. Rev.* **1950**, *80*, 72−80.

(27) Qiao, J.; Kong, X.; Hu, Z.-X.; Yang, F.; Ji, W. High-mobility transport anisotropy and linear dichroism in few-layer black phosphorus. *Nat. Commun.* **2014**, *5*, 4475.

(28) Landauer, R. Spatial v of currents and fields due to localized scatterers in metallic conduction. *IBM J. Res. Dev.* **1957**, *1*, 223−231.

(29) Büttiker, M. Four-terminal phase-coherent conductance. *Phys. Rev. Lett.* **1986**, *57*, 1761−1764.

(30) Marini, A.; Hogan, C.; Grüning, M.; Varsano, D. Yambo: An ab initio tool for excited state calculations. *Comput. Phys. Commun.* **2009**, *180*, 1392−1403.

(31) Henkelman, G.; Arnaldsson, A.; Jónsson, H. A Fast and Robust Algorithm for Bader Decomposition of Charge Density. *Comput. Mater. Sci.* **2006**, *36*, 354−360.

(32) Ma, Y.; Kuc, A.; Heine, T. Single-layer Tl_2O: a metal-shrouded 2D semiconductor with high electronic mobility. *J. Am. Chem. Soc.* **2017**, *139*, 11694−11697.

(33) Mak, K. F.; Lee, C.; Hone, J.; Shan, J.; Heinz, T. F. Atomically thin MoS_2: a new direct-gap semiconductor. *Phys. Rev. Lett.* **2010**, *105*, 136805.

(34) Splendiani, A.; Sun, L.; Zhang, Y.; Li, T.; Kim, J.; Chim, C.-Y.; Galli, G.; Wang, F. Emerging photoluminescence in monolayer MoS_2. *Nano Lett.* **2010**, *10*, 1271−1275.

(35) Cai, Y.; Zhang, G.; Zhang, Y.-W. Polarity-reversed robust carrier mobility in monolayer MoS_2 nanoribbons. *J. Am. Chem. Soc.* **2014**, *136*, 6269−6275.

(36) Xi, J.; Long, M.; Tang, L.; Wang, D.; Shuai, Z. First-principles prediction of charge mobility in carbon and organic nanomaterials. *Nanoscale* **2012**, *4*, 4348−4369.

(37) Bruzzone, S.; Fiori, G. Ab-initio simulations of deformation potentials and electron mobility in chemically modified graphene and two-dimensional hexagonal boron-nitride. *Appl. Phys. Lett.* **2011**, *99*, 222108.

(38) Zhou, L.-J.; Zhang, Y.-F.; Wu, L.-M. SiC_2 siligraphene and nanotubes: Novel donor materials in excitonic Solar Cells. *Nano Lett.* **2013**, *13*, 5431−5436.

(39) Dong, H.; Zhou, L.; Frauenheim, T.; Hou, T.; Lee, S.-T.; Li, Y. SiC_7 siligraphene: A novel donor material with extraordinary sunlight absorption. *Nanoscale* **2016**, *8*, 6994−6999.

(40) Zhou, L.; Zhang, J.; Zhuo, Z.; Kou, L.; Ma, W.; Shao, B.; Du, A.; Meng, S.; Frauenheim, T. Novel Excitonic Solar Cells in Phosphorene-TiO_2 Heterostructures with Extraordinary Charge Separation Efficiency. *J. Phys. Chem. Lett.* **2016**, *7*, 1880−1887.

(41) Bernardi, M.; Palummo, M.; Grossman, J. C. Extraordinary sunlight absorption and one nanometer thick photovoltaics ssing two-dimensional monolayer materials. *Nano Lett.* **2013**, *13*, 3664−3670.

(42) Kistanov, A. A.; Cai, Y.; Zhou, K.; Dmitriev, S. V.; Zhang, Y.-W. The role of H_2O and O_2 molecules and phosphorus vacancies in the structure instability of phosphorene. *2D Mater.* **2017**, *4*, No. 015010.

DOI: 10.1021/acs.jpclett.8b03077
J. Phys. Chem. Lett. 2018, 9, 6915−6920